Inhalational delivery of induced pluripotent stem cell secretome improves postpneumonectomy lung structure and function

D. Merrill Dane[1], Khoa Cao[1], Yu-An Zhang[1], Kemp Kernstine[2], Amiq Gazdhar[3,4], Thomas Geiser[3,4], and Connie C.W. Hsia[1]

[1]Departments of Internal Medicine and [2]Cardiothoracic Surgery, University of Texas Southwestern Medical Center, Dallas, TX.

[3]Depts. of Pulmonary Medicine and [4] Biomedical Research, University of Bern, Switzerland

Running title: Inhalational iPSC secretome treatment post-pneumonectomy

Supported by NHLBI R01 HL134373 and U01 HL111146 (C.C.W.H), and the Swiss National Science Foundation SNF 310030_141102 (T.G.)

Address correspondence to:

Connie C.W. Hsia, MD
Pulmonary & Critical Care Medicine
Dept. of Internal Medicine
University of Texas Southwestern Medical Center
5323 Harry Hines Blvd.
Dallas, TX 75390-9034
TEL: 214-648-3426
Email: Connie.Hsia@utsouthwestern.edu

Abstract

Cell-free secretory products (secretome) of human induced pluripotent stem cells (iPSCs) have been shown to attenuate tissue injury and facilitate repair and recovery. To examine whether iPSC secretome facilitates mechanically-induced compensatory responses following unilateral pneumonectomy (PNX), litter-matched young adult female hounds underwent right PNX (removing 55-58% of lung units) followed by inhalational delivery of either the nebulized conditioned media containing iPSCs secretome (iPSC CM) or control cell-free media (CFM); inhalation was repeated every 5 days for 10 treatments. Lung function was measured under anesthesia pre-PNX and 10 d after the last treatment (8 weeks post-PNX); detailed quantitative analysis of lung ultrastructure was performed postmortem. Pre-PNX lung function was similar between groups. Compared to CFM control, treatment with iPSC CM attenuated the post-PNX decline in DL_{CO} and DM_{CO}, accompanied by a 24% larger postmortem lobar volume and distal air space enlargement. Alveolar double-capillary profiles were 39% more prevalent consistent with enhanced intussusceptive angiogenesis. Frequency distribution of the harmonic mean thickness of alveolar blood-gas barrier shifted towards the lowest values while alveolar septal tissue volume and arithmetic septal thickness were similar, indicating septal remodeling and reduced diffusive resistance of the blood-gas barrier. Thus, repetitive inhalational delivery of iPSC secretome enhanced post-PNX alveolar angiogenesis and septal remodeling that are associated with improved gas exchange compensation. Results highlight the plasticity of the remaining lung units following major loss of lung mass that are responsive to broad-based modulation provided by the iPSC secretome.

Key words: induced pluripotent stem cells, secretome, compensatory lung growth, alveolar remodeling, lung diffusing capacity.

Noteworthy:

To examine whether the secreted products of human induced pluripotent stem cells (iPSC) facilitate innate adaptive responses following loss of lung tissue, adult dogs underwent surgical removal of one lung, then received repeated administration of iPSC secretory products via inhalational delivery compared to control treatment. Inhalation of iPSC secretory products enhanced capillary formation and beneficial structural remodeling in the remaining lung, leading to improved lung function.

Introduction

Major lung resection by pneumonectomy (PNX) mimics the consequences of destructive lung disease regardless of specific etiology and is a useful model for studying the mechanisms and adaptive potential of the remaining functioning units. Following right PNX, the markedly increased supra-threshold mechanical stresses on the remaining lung units result in vigorous expansion and compensatory alveolar tissue-capillary growth (5, 7, 37, 38), leading to balanced generation of new acinar structural components, progressive remodeling of existing structure, and eventually augmentation of lung function. Robust post-PNX responses have been documented in multiple species and in both young and adult animals (18); compensation is more complete in young than adult animals, suggesting a need for exploring interventions to amplify the innate response and fully harness the potential plasticity in the adult lung. In the presence of sufficient mechanical signals, active compensatory responses may be pharmacologically augmented; supplementation with individual growth promoters in adult canines enhanced selected aspects of post-PNX structural growth, angiogenesis and acinar and alveolar septal remodeling but not global lung function (4, 6, 34, 51). This "*structure-function gap*" in response may be the result of a) supra-physiologic and/or skewed pharmacological stimulation, b) inadequate tissue protection from mechanically-induced oxidative stress damage and c) inadequate architectural remodeling. These considerations suggest a need for a broad panel of factors such as those produced by stem cells capable of modulating the myriad homeostatic pathways involved in a balanced interactive response, to maximize the innate potential for compensation and improve lung function.

The role of stem cells during post-PNX compensation remains poorly understood (26, 30). In addition to alveolar type-2 epithelial cells classically considered to be progenitors, putative distal airway progenitor cells also increase in number post-PNX (9) and exhibit age-related proliferative and reparative potential (31). Delivery of exogenous stem cells including induced

pluripotent stem cells (iPSCs) has been reported to alleviate acute lung injury and facilitate repair and regrowth (3, 11, 15, 29, 42, 47, 53). However, in vivo delivery of intact stem cells has been limited by a low rate of engraftment and retention, and risks of immunogenicity and tumorigenicity (1, 16, 45). Instead, the modest beneficial effects of stem cell delivery are thought to be mediated mainly through the production of growth factors, cytokines, exosomes and microvesicles, that constitute the secretome (2); therefore, an alternative approach is targeted local delivery of cell-free conditioned media (CM) containing the stem cell secretome. We have shown that tracheal delivery of iPSC CM containing the secretome alleviated bleomycin- and hyperoxia-induced acute lung injury (10, 11); treatment activated endogenous antioxidant proteins, enhanced antioxidant capacity and ameliorated oxidative damage to DNA, lipid, and protein (11).

Based on the above observations, we hypothesized that pulmonary delivery of cell-free iPSC secretome protects lung tissue from damage arising from post-PNX mechanical stress and facilitates compensatory growth and remodeling, leading to enhanced function of the remaining lung. To test this hypothesis and establish the feasibility of pulmonary delivery of stem cell products in a large animal model, we nebulized the CM containing well-characterized iPSC secretome (10, 11) for repeated inhalational delivery into the lungs of adult canines over ~8 weeks following right PNX. Control animals received cell-free media (CFM) in a similar fashion. Blood oxidative damage markers and lung function were measured before and after PNX, and detailed postmortem lung morphometry was performed. Results show that inhalation of iPSC secretome enhanced post-PNX alveolar angiogenesis and septal remodeling, leading to reduced alveolar-capillary diffusion resistance and improved diffusing capacity in the remaining lung.

Methods

Animals and experiments The Institutional Animal Care and Use Committee of the University of Texas Southwestern Medical Center approved all procedures. Litter-matched young adult mixed-breed female hounds (total n=13, 10 months old, body weight 18.3 ± 1.1 kg, mean ± SD), were obtained from approved vendor (Marshall Farms, Rose, NY). A flowchart of experimental design is shown in **Figure 1**.

Right pneumonectomy Following completion of baseline (pre-PNX) measurements, the animal underwent right PNX following established procedures (5, 7). Briefly, the animal was premedicated, anesthetized, intubated, and mechanically ventilated. Rectal temperature, heart rate, blood pressure, and transcutaneous O_2 saturation were continuously monitored. Through a small right lateral fifth intercostal space thoracotomy, individual hilar vessel ligation and stapling of the bronchus was performed, covering the bronchus by oversewing adjacent healthy regional tissue. The bronchial stump was checked for leaks and then oversewn with loose hilar tissue for added protection. Lidocaine (1%) was applied to the intercostal nerves and the chest wall closed in layers. Residual thoracic air was evacuated to underwater seal. Supplemental O_2 was administered as needed. Intraoperative fluid administration was minimized (<50 mL). Analgesia (Buprenorphine) was administered postoperatively for 48 h and then as needed. The animal was monitored daily; skin stitches were removed in 7–10 days. The remaining left lobes were estimated to comprise on average 42% of the pre-PNX total lung volume (38).

iPSC conditioned media Production of iPSC CM followed established procedures (10, 11). Human foreskin dermal fibroblasts were reprogrammed into iPSCs using established protocols (10). For producing the cell-free iPSC conditioned media (CM), iPSCs ($1x10^6$) were grown in Corning ultra-low attachment flask ($75cm^2$); once the cells formed spheres the culture media was changed to a serum free media without additional supplements and the cells were grown for 24 hours. Cell-free CM containing the iPSC secretome was harvested and characterized,

133 then kept deeply frozen (-80ºC) until use. An aliquot (10 mL) was defrosted (4ºC) overnight and
134 gently vortexed before use. Control cell-free media (CFM) was similarly processed.

135 *Inhalational delivery* Following PNX and chest wall closure, animals received the nebulized
136 compound (iPSC CM or CFM) before recovery from anesthesia; subsequent treatments were
137 given every 5 days for a total of 10 treatments. For each treatment (6), the animal was fasted
138 overnight and premedicated with acepromazine (0.05 mg/kg IM) and atropine (0.04 mg/kg IM).
139 Anesthesia was induced with propofol (4 mg/kg IV) and maintained with propofol as needed
140 (approximately 0.5-1.0 ml/min). Each animal was intubated and mechanically ventilated in the
141 supine position (16-18 breaths/min, 50/50 inspiration/expiration ratio, tidal volume 10-12 ml/kg).
142 Mouth pressure, O_2 saturation and heart rate were monitored. The animal pre-breathed 100%
143 oxygen in an open circuit for 1-2 min and then were switched to a closed circuit connected to a
144 reservoir bag and a nebulizer (Aerogen Aeroneb Pro, Tri Anim, Sylmar CA). The desired media
145 (10 mL) was nebulized (4 μm droplets) into the inspiratory limb of the breathing circuit and
146 delivered via the tracheal tube (average flow rate 0.4 mL/min, minimum flow rate 0.2 mL/min),
147 followed by nebulization of two 1 mL saline rinses to ensure complete delivery. Oxygen was
148 added to the circuit as needed to keep O_2 saturation above 90%. The entire procedure was
149 complete in 20-30 min.

150 *Biochemical assays* Peripheral venous blood (2 mL each) was collected before, during, and
151 after the first two treatments and then at every other treatment. Plasma was used for
152 measurement of oxidative stress markers 8-hydroxy-2'-deoxyguanosine (8-OHdG, Cell Biolabs,
153 San Diego, CA) and 8-isoprostane (Cayman Chemical, Ann Arbor, MI). Serum was used for
154 measurement of total antioxidant capacity (OxiSelect STA-360, Cell Biolabs). Complete blood
155 counts and biochemical panels (Superchem + CBC) were measured pre-PNX and at 1 h, 5 d,
156 30 d and 55 d post-PNX.

157 *Physiological studies* Lung function was measured pre-PNX and 55 d post-PNX (10 d
158 after completion of inhalation treatments) (6, 7). The animal was fasted overnight, pre-
159 medicated with acepromazine (0.05 mg/kg IM) and atropine (0.04 mg/kg IM). Anesthesia was
160 induced with propofol (4 mg/kg IV) and maintained with intravenous ketamine and diazepam
161 infusion at a dose titrated to effect. Animal was intubated with a cuffed endotracheal tube and
162 mechanically ventilated supine (tidal volume 10-12 ml/kg, 16-18 breaths/min) to eliminate
163 spontaneous breathing effort. Rectal temperature, heart rate, transcutaneous O_2 saturation, and
164 mouth and esophageal pressures, were monitored. Static transpulmonary pressure-lung volume
165 (PV) curves were measured using a calibrated syringe inflating the lungs to 15, 30 ,45, and 60
166 ml/kg above end-expiratory lung volume (EELV), or up to a transpulmonary pressure of 30 cm
167 H_2O, in increasing and then decreasing order. End-inspiratory and end-expiratory lung volume
168 (EILV), pulmonary blood flow, lung diffusing capacity for carbon monoxide (DL_{CO}) and nitric
169 oxide (DL_{NO}), and septal tissue (including microvascular blood) volume were measured
170 simultaneously using an established rebreathing technique (4, 23) at two inspired O_2
171 concentrations (21% and 99%) and a lung volume of 45 ml/kg above EELV. The components of
172 DL_{CO}: membrane diffusing capacity (DM_{CO}) and pulmonary capillary blood volume (V_c), were
173 calculated from DL_{CO} measurements obtained at the two alveolar O_2 levels using established
174 methods (19, 39). Duplicate measures under each condition were averaged. PV curves were
175 analyzed using established methods (32, 41). Specific lung compliance was calculated from the
176 changes in lung volume and transpulmonary pressure between 10 and 30 cm H_2O and
177 normalized by the lung volume at 10 cm H_2O.

178 *Lung fixation* Under deep anesthesia, a tracheostomy was performed; a cuffed endotracheal
179 tube was inserted and tied securely. The chest was opened via a left lateral thoracotomy. An
180 overdose of pentobarbital (120 mg/kg IV) was administered and the remaining lung re-inflated
181 within the thorax by tracheal instillation of 2.5% buffered glutaraldehyde at a hydrostatic

182 pressure of 25 cmH_2O above the sternum. After the flow of fixative ceased, the tracheal tube
183 was closed to maintain airway pressure. The lungs were removed intact, immersed in buffered
184 2.5% glutaraldehyde, floated on a water bath, and stored at 4°C for at least 4 weeks before
185 processing.

186 *Lung morphometry* Volume of the left caudal lobe was measured by saline immersion; then
187 the lobe was serially sectioned (2 cm thickness). Volume of the sectioned stress-free lobe was
188 measured using the Cavalieri Principle, an established method of measuring the volume of
189 irregularly shaped objects. The total area of serial slices is estimated by point counting, then
190 multiplied by slice thickness to yield lobe volume (52). An unbiased systematic random sampling
191 scheme was used to select 8 blocks per lobe (21). Sectioned slices were arranged on a tray in
192 the same orientation with a grid overlay. From a random start, tissue samples (1.5 cm in each
193 dimension) were systematically selected at a fixed interval along grid points (4 each at
194 subpleural and interior locations). Tissue blocks were post-fixed with 1% osmium tetroxide in
195 0.1M cacodylate buffer, treated with 2% uranyl acetate, dehydrated through graded alcohol, and
196 embedded in Spurr resin (Electron Microscopy Sciences, Hartfield, PA). The other remaining
197 lobes were processed separately for other studies.

198 An established stratified analytical scheme (21) was used under low and high power light
199 microscopy (LM; 275x and 550x) and transmission electron microscopy (TEM; ~16,000x). For
200 LM, each block was sectioned (1μm) and stained (toluidine blue). One section per block was
201 overlaid with a test grid. At 275x, at least 20 non-overlapping fields were systematically sampled
202 from a random start. Excluding the structures between 20 μm and 1 mm in diameter; the volume
203 densities of fine parenchyma, alveolar sac and alveolar duct were estimated using point
204 counting. At 550x, at least 20 non-overlapping fields were systematically sampled to estimate
205 the volume density of alveolar septa. For TEM, each block was sectioned (70 nm) and mounted
206 on copper grids. Each grid was examined at ~16,000x (JEOL EXII). At least 30 non-overlapping

fields per grid were systematically sampled. Volume densities of epithelium type I and II, interstitium, endothelium and capillaries were estimated using point counting with alveolar septum as the reference space. Surface densities of alveolar epithelial and capillary were estimated using intersection counting (21). At least 300 points or intersections were counted per grid. Harmonic mean barrier thickness of the blood-gas barrier (τ_{hb}) was measured from the lengths of intercept lines between alveolar surface and erythrocyte membrane.

Absolute volumes and surface areas of individual structures were calculated from the products of fractional quantities estimated at each level. Prevalence of double capillary profiles, an index of intussusceptive capillary formation (8, 22, 38), was calculated by completely sampling 2 grids under TEM (~2,500x) and expressed as a ratio of (double capillaries)/(total number of capillaries).

Statistical analysis Results (mean±SD) were normalized by body weight where appropriate. Pressure-volume curves and temporal changes (pre- to post-PNX) between treatment groups were compared by factorial and/or repeated measures ANOVA with post hoc test by Fisher's protected least significant difference (STATVIEW v.5.0). Morphometric parameters were compared between groups by unpaired t test. A p value ≤0.05 was considered significant.

Results

One animal in in iPSC CM group died from acute post-operative pulmonary bleeding; one animal in CFM group was terminated due to post-operative vomiting and weight loss. The remaining 11 animals (6 iPSC CM, 5 CFM) completed the study without complications. Physiological data are summarized in **Table 1 and Figures 2-3**. Body weight, systemic hematocrit and pre-PNX lung function were similar between groups (**Table 1**). In both groups, post-PNX static lung volume at a given transpulmonary pressure was lower (**Figure 2**) while specific lung compliance was similarly unchanged compared to pre-PNX (**Table 1**). During

231 rebreathing, mean alveolar O_2 tension and septal tissue volume were unchanged pre- to post-
232 PNX. Mean lung volumes were similarly maintained post-PNX in both groups (**Figure 3A-B**).
233 Pulmonary blood flow decreased post-PNX in CFM group and changed variably in iPSC CM
234 group (**Figure 3C**). Post-PNX DL_{CO} declined in both groups; the magnitude of decline from pre-
235 PNX in iPSC CM group (29%) was attenuated compared to that in the CFM group (48%,
236 p=0.026) by paired analysis (**Figure 3D**). In a similar pattern, DM_{CO} declined pre- to post-PNX in
237 CFM group (42%, p=0.04) whereas the post-PNX decline in iPSC CM group was less and not
238 significantly different from pre-PNX (14%, p=0.19) (**Figure 3E**). Baseline Vc was highly variable
239 in CFM group and pre-to-post-PNX paired comparison did not reach significance (p=0.19)
240 (**Figure 3F**). In iPSC group, pre-PNX Vc was less variable and declined consistently post-PNX
241 (p=0.03). The average Vc magnitude did not differ significantly between groups pre- or post-
242 PNX (p=0.15 and 0.44, respectively) and the average decline (post/pre-PNX ratio) also did not
243 differ (0.68 vs. 0.60 in CFM and iPSC groups, respectively, p=0.69).

244 Plasma oxidative damage markers and total antioxidant capacity (**Figure 4A to 4C**) increased
245 post-operatively then declined at different rates. Plasma 8-OHdG, a marker of DNA oxidative
246 damage, steadily increased up to four-fold post-PNX, peaking around day 10 then slowly
247 declined but still remained elevated at 55 d (**Figure 4A**). Plasma 8-isoprostane, a marker of lipid
248 oxidation, increased only mildly post-PNX then declined below pre-PNX baseline (**Figure 4B**).
249 Total antioxidant capacity also increased modestly post-PNX then returned to baseline in ~10
250 days. At this arbitrary secretome dose these profiles did not differ significantly between
251 treatment groups.

252 Morphometric results are available in 5 animals per group (**Tables 2-4** and **Figures 5-7**). The
253 lung from one animal (iPSC CM group) was excluded due to inadequate inflation and fixation. In
254 the iPSC CM group, volume of the remaining left caudal lobe was 26% larger ($p<0.05$)
255 compared to the control group (p=0.04) due to larger alveolar ducts and sacs (**Table 2, Figure**

256 **6A-6B**) as shown by representative micrographs (**Figure 5**). Volume and surface densities
257 (**Table 3**) and absolute volumes and surface areas (**Table 4**) of septal tissue and capillary
258 components did not differ between groups. With iPSC the alveolar surface area was 21% higher
259 but did not reach statistical significance (p=0.09) (**Table 3, Figure 6C**). The prevalence of
260 double capillary profiles was significantly (39%) higher in the iPSC CM group (p=0.006) (**Table**
261 **4, Figure 6D**), consistent with enhanced intussusceptive capillary formation. The frequency
262 distribution of harmonic mean blood-gas barrier thickness (τ_{hb}) shifted significantly towards the
263 lowest value category (**Figure 7**), suggesting remodeling and re-arrangement of septal
264 constituents and reduced barrier resistance to diffusion while the arithmetic thickness of alveolar
265 septum was similar between groups (**Table 2**). The combined results indicate larger volume and
266 air spaces, enhanced intussusceptive alveolar capillary formation, and septal remodeling that
267 reduced barrier resistance to diffusion in secretome-treated lungs. These changes are
268 associated with a 25% higher estimated morphometric diffusing capacity of the tissue-plasma
269 barrier (DB_{O2}) (p=0.068) (**Table 4**) and correspond to the better preservation of post-PNX whole
270 lung DL_{CO} measured by a physiological method (**Figure 3D**).

271 **Discussion**

272 *Summary of the main findings* This is the first report to establish the feasibility and
273 efficacy of inhaled iPSC-derived cell-free secretome for enhancing post-PNX compensation in a
274 large animal model. Pre-PNX lung function was similar between groups. Post-PNX plasma 8-
275 OHdG level remained elevated for 55 d post-PNX, indicating persistent DNA oxidative stress
276 while plasma 8-isoprostane and total antioxidant capacity levels increased mildly and
277 transiently; the temporal profiles did not differ between groups at this treatment dose. In
278 secretome-treated compared to control animals, physiologic whole lung volume measured at
279 near total lung capacity was similar. However, postmortem stress-free volume of the caudal lobe
280 was 26-30% larger in secretome-treated animals. Differences between antemortem and

281 postmortem volumes suggest dynamic extra-pulmonary factors, e.g., thoracic and/or
282 diaphragmatic restriction, that limited lung expansion in the living animal. Secretome-treated
283 animals exhibited increased intussusceptive alveolar angiogenesis (double capillaries) and
284 septal remodeling with enlarged terminal airspaces and reduced barrier resistance to diffusion;
285 absolute alveolar surface area was also higher without reaching statistical significance. These
286 structural changes resulted in a 25% higher conductance of the blood-gas barrier (borderline
287 significance), which is consistent with physiological findings of better preservation of DM_{CO} and
288 a 23% higher physiologic DL_{CO} in post-PNX animals treated with iPSC CM. We conclude that
289 repetitive inhalational delivery of iPSC secretome enhanced endogenous post-PNX
290 angiogenesis and acinar and alveolar septal remodeling leading to modest and significant
291 improvement in gas exchange compensation. These findings highlight the plasticity of adult lung
292 units that remain following destructive processes and the responsiveness of these units to
293 broad-based modulation provided by iPSC secretome.

294 *Critique of the methods* Both iPSCs (10, 11, 33, 44) and mesenchymal stem cells (MSCs)
295 (12, 27-29, 49) or their secretome possess injury-alleviating and tissue regenerative potential. A
296 Phase I trial of systemic infusion of allogenic MSCs on aging frailty showed promising results
297 compared to placebo (13); however, more studies are needed in this and other conditions. Here
298 we chose to test a cell-free iPSC secretome preparation for enhancing post-PNX compensation;
299 the preparation has been characterized and shown to alleviate experimental lung injury (10, 11,
300 44). The iPSCs may be derived from readily available sources, e.g., human dermal fibroblasts,
301 and can differentiate into a variety of cell types including organ-specific MSCs (43). Other cell
302 types, e.g., fibroblasts, may secrete some of the same ingredients but lack the overall injury-
303 alleviating capacity of iPSCs (10, 11). There are no direct comparisons between iPSCs and
304 MSCs for post-PNX compensation; this comparison is beyond the scope of our report but may
305 be pursued in the future. The inhalational approach (6) and physiologic and morphometric

306 assessment (21) are established. An earlier canine study of post-PNX inhalation treatment of
307 exogenous erythropoietin documented the delivery of exogenous protein to the caudal lobe (6)
308 and showed that alveolar septal changes and the magnitude of enhancement of angiogenesis
309 were comparable among all post-PNX remaining lobes; structural response in the caudal lobe
310 was representative of that of the remaining lung (6, 7). In the current study, the largest
311 remaining lobe (left caudal, ~55% of total left lung volume) was sampled for morphometry. Both
312 subpleural and central lobar regions were sampled.

313 The derived components of DL_{CO} (DM_{CO} and Vc) are interdependent quantities that typically
314 exhibit larger variability than DL_{CO}. In CFM group post-PNX DM_{CO} declined 42% ($p=0.04$ vs. pre-
315 PNX) whereas in iPSC CM group the decline was less (14%) and the pre-to-post-PNX paired
316 values were not significantly different ($p=0.19$), suggesting that iPSC CM minimized post-PNX
317 decline in DM_{CO}, i.e., a similar pattern as DL_{CO}. Vc is sensitive to hemodynamic fluctuations,
318 exhibiting a variable baseline in CFM group that hampered inter-group comparisons.
319 Nevertheless, post-PNX Vc was less variable and reached similar levels in both groups
320 consistent with morphometric results where the average postmortem alveolar capillary blood
321 volume also did not differ significantly between groups ($p=0.82$) (**Table 4**). Variability in baseline
322 Vc does not alter the conclusion that DL_{CO}, the primary measure of diffusive gas exchange, was
323 better preserved in post-PNX animals treated with iPSC CM.

324 Two plasma biomarkers, 8-isoprostane and 8-OHdG, that reflect oxidative stress damage to
325 lipid and DNA, respectively, and are known to increase post-PNX (6), were measured along with
326 total antioxidant capacity. Plasma 8-OHdG was persistently elevated at 55 d post-PNX (**Figure**
327 **4A**), indicating ongoing DNA oxidative stress most likely related to the still increased mechanical
328 stresses on the remaining lung. Pulmonary delivery of iPSC secretome attenuates oxidative
329 damage in acute hyperoxic lung injury (11); a higher dose or more frequent dosing may be
330 needed to attenuate persistent post-PNX mechanically induced oxidative stress. The optimal

dose-response relationships remain to be determined. Treatment duration (~8 weeks) spanned the early post-PNX period marked by active cell proliferation and matrix deposition; progressive architectural remodeling and further gains in lung function continue well beyond this period (20, 55, 56). Therefore, a longer period of therapy and monitoring will be needed to assess the ultimate outcome. Physiological assessment was made under anesthesia; the responses while awake or during exercise may differ. This study used female animals; sex differences in response to PNX are largely explained by body size (Dane, Kernstine, Hsia, unpublished data). Further studies will be required to determine any sex differences in response to iPSC secretome treatment.

Mechanically induced post-PNX lung growth and remodeling Post-PNX increases in lung volume, perfusion and blood volume of the remaining lobes transduce compensatory responses (5, 7, 37, 59). We previously documented a threshold, optimal range and upper limit of post-PNX compensatory response, summarized in (38). Following left PNX (42% of lung units removed), most of the remaining lobes compensated via recruitment of existing alveolar-capillary reserves without new tissue growth, except the right infracardiac lobe that underwent the largest expansion across the midline anterior and caudal to the cardiac fossa with nearly two-fold increases in tissue-capillary volumes. Following right PNX (58% resection), mechanical stress on the remaining lobes exceeded a growth-stimulating threshold and all the remaining lobes exhibited 2 to 2.5 fold increase in alveolar septal components. Following bilateral resection removing up to 70% of lung units (~35% each side) the remaining lobes exhibited significant though diminished alveolar-capillary growth than that after 58% resection, suggesting that an optimal stimulus-response range was exceeded.

Interventions to augment compensatory lung growth Attempts to enhance innate post-PNX responses using individual growth promoters in rodent models led to mixed cellular and structural effects (14, 24, 25, 40, 57) and few studies assessed the functional outcome on gas

exchange. In our earlier canine studies (4, 6, 34, 51, 54), oral *all-trans* retinoic acid significantly enhanced active alveolar re-growth after right PNX (34, 51) but had no effect after left PNX (50), suggesting that pharmacological agents modify active mechanically-induced lung growth but cannot re-initiate growth de novo in the absence of sufficient mechanical stimuli. Delivery of retinoic acid or recombinant erythropoietin enhanced post-PNX alveolar double-capillary formation, consistent with the notion of intussusceptive angiogenesis as an essential event in compensatory lung growth (22). Retinoic acid augmented post-PNX volumes of alveolar type-1 epithelium, interstitial collagen and matrix, endothelium and pulmonary capillary blood, but the volume increase in type-2 epithelium lagged behind; structural distortion developed with thicker alveolar septa and basement membrane and smaller air spaces indicating inadequate remodeling (4, 34, 51). Erythropoietin possesses potent cytoprotective and pro-angiogenic properties; inhaled recombinant human erythropoietin improved post-PNX in vivo distribution of pulmonary blood flow (54) and abrogated oxidative stress damage (6), but exerted only minor effects on extravascular alveolar tissue compartments. In spite of enhancing certain aspects of the post-PNX response, neither of the above agents augmented lung function above that in vehicle-treated post-PNX control animals. This "*structure-function gap*" in response to pharmacological intervention is not surprising as each agent can stimulate only a subset of interacting growth-related pathways, and may elicit supra-physiologic responses causing distortion at micro- and macro-scopic levels. Furthermore, the selective structural alterations were not accompanied by appropriate acinar or alveolar septal remodeling to optimize gas exchange efficiency. This structure-function gap provides rationale for a cocktail approach such as that offered by the iPSC secretome consisting of a broad panel of counter-acting mediators capable of supporting balanced modulation of post-PNX adaptation without distortion to ultimately attain functional benefit.

The iPSC secretome Delivery of stem cell secretome has been called an empirical "*shotgun*" approach; yet this approach directly and mechanistically addresses the pre-requisite for useful lung growth and remodeling leading to functional compensation, i.e., the need for balanced physiologic modulation of all relevant mediator pathways and gas exchange structures with minimal distortion. Few studies focused on iPSC secretome; our preparation has been characterized by proteomic analysis, and found to contain >1,200 proteins (10, 11) including a markedly enriched αKlotho content (10-25 fold of that in normal serum). αKlotho is an essential cell maintenance and cytoprotective protein with pleiotropic actions including anti-apoptosis and potent antioxidation via activation of the nuclear factor (erythroid 2)-related factor 2 (Nrf2) network of endogenous antioxidant proteins (11, 35, 36). The lung normally does not express αKlotho (58) but depends on kidney-derived circulating αKlotho for cytoprotection (35, 36). Immunodepletion of αKlotho from iPSC CM reduced in vitro cytoprotective effects of iPSC CM by ~50% (11). Tracheal delivery of this secretome preparation alleviated bleomycin and hyperoxia induced acute lung injury compared to fibroblast conditioned media (10, 11), enhanced total antioxidant capacity, ameliorated oxidative damage to DNA, lipid, and protein, and broadly activated endogenous antioxidant proteins (11). Others reported that iPSCs or their secretory products reduced pro-inflammatory and pro-fibrotic cytokines and chemokines (17) and iPSC-derived exosomes/microvesicles protected against cardiac ischemia/reperfusion injury (46). Gene network analysis of lung interstitial macrophages from bleomycin-injured rats treated with this secretome preparation demonstrated modulation of multiple pathways involved in immunomodulation, branching morphogenesis and canonical Wnt signaling (44). Our data support the benefit of *intact iPSC secretome* in modulating the manifold adaptive mechanisms required for compensatory alveolar angiogenesis and remodeling to facilitate more efficient diffusive gas exchange. iPSC-derived cytoprotective factors such as αKlotho may have permitted fuller expression of the innate compensatory potential of the remaining lung.

Comparisons between the single-agent and our broad-based interventional approaches offer several useful insights:

1) Pharmacological augmentation of the formation of new alveolar tissue-capillary elements alone is insufficient for achieving functional benefit unless the increase in these elements is accompanied by appropriate architectural remodeling to optimize gas exchange.

2) Since lung growth and regeneration involve multiple dynamic processes, a broad-based cocktail approach is superior to single or a few agents for bridging the structure-function gap in attempts to amplify innate adaptive responses. This general concept is analogous to the "cocktail" therapy routinely used in cancer chemotherapy to broadly target the myriad factors that promote tumor growth and spread.

3) Individual secretome-induced structural modulations may be modest or borderline significant, but assume cumulative significance with respect to global lung function. For example, the 5% lower ($p<0.05$) average harmonic mean barrier thickness (τ_{hb}) in secretome-treated lungs was due to a preferential shift in the frequency distribution of τ_{hb} to the thinnest part of the barrier (a 9% increase, $p=0.02$, **Figure 7**). This modest shift disproportionally increases gas transfer efficiency, because alveolar gas conductance is proportional to the reciprocal of τ_{hb} (48) and >90% of alveolar gas exchange takes place across the thinnest part of the septa while the thicker parts mainly provide physical support. Combined with the 17-20% higher ($p=0.09$) alveolar-capillary surface areas, these changes could account for a 25% higher morphometric estimate of barrier conductance ($p=0.068$) and a 23% higher physiologic DL_{CO} ($p=0.04$) in animals treated with iPSC CM compared to CFM over ~8 weeks. These are very reasonable rates of improvement considering the need to maintain balanced structure-function responses and minimize distortion throughout all regions of a large stratified lung.

Conclusions Previous attempts to amplify post-PNX compensatory responses were partially successful but identified an important challenge of *structure-function dissociation*, i.e., individual exogenous growth promoters augmented selective aspects of tissue-capillary growth but not architectural remodeling or functional outcome. We report here that inhalation of a well-characterized cell-free iPSC secretome preparation overcame this dissociation by enhancing post-PNX angiogenesis and alveolar remodeling leading to more efficient gas exchange. These novel findings reinforce the concept that post-PNX compensation is a highly orchestrated multi-phasic process involving myriad pathways and mediators many of which are not classically considered to be growth promoters. In addition to mechanically stimulated cell proliferation and tissue-capillary growth, progressive structural remodeling minimized resistance of the diffusion barrier, a critical requirement for achieving functional compensation. Innate post-PNX compensation may be augmented by supplementing with iPSC secretome composed of broad-based mediators in a physiologically relevant cocktail. These results established the feasibility and efficacy of inhalational delivery of iPSC secretome in the canine model.

Many aspects of this emergent approach require further investigation, including characterization and optimization of secretome composition and bioactivity, elucidation of the mechanisms of action and interaction among the components, and determination of the degrees to which the major components contribute to the observed effects. Our premise is that the *entire secretome* is responsible for coordinated enhancement of post-PNX angiogenesis and remodeling required for translating post-PNX tissue growth into functional gain; future studies may compare intact secretome with subfractions such as exosomes and microvesicles. Unlike the short-term use of secretome in acute lung injury, the post-PNX remaining lung undergoes progressive remodeling over many months with gradual functional improvement (56), and may be susceptible to secretome action throughout this period as the existing acinar scaffold is slowly modified. Therefore, sustained modest and balanced modulation is preferable to acute supra-physiologic

skewed stimulation. Prolonged secretome therapy may be needed to maximize long-term structural and functional gain and facilitate realization of the full innate compensatory potential. Measurement of lung function during exercise may accentuate treatment effects. Impact of the secretome delivery approach extends beyond the PNX model to regenerative therapy for parenchymal lung diseases irrespective of the specific etiology.

Acknowledgement

We thank Dr. Matthew Riegel, DVM, and the staff of the Animal Resources Center at UT Southwestern for veterinary assistance, and Anna-Barbara Tschirren at University of Bern for technical assistance. This work was supported by National Heart, Lung and Blood Institute grants R01-HL134373 and U01-HL111146 (CCWH), and the Swiss National Science Foundation (SNF 310030_141102) (TG).

Conflict of interest

The authors have no conflict of interest to declare.

References

1. **Abad M, Mosteiro L, Pantoja C, Canamero M, Rayon T, Ors I, Grana O, Megias D, Dominguez O, Martinez D, Manzanares M, Ortega S, and Serrano M**. Reprogramming in vivo produces teratomas and iPS cells with totipotency features. *Nature* 502: 340-345, 2013.

2. **Abman SH, and Matthay MA**. Mesenchymal stem cells for the prevention of bronchopulmonary dysplasia: delivering the secretome. *Am J Respir Crit Care Med* 180: 1039-1041, 2009.

3. **Asmussen S, Ito H, Traber DL, Lee JW, Cox RA, Hawkins HK, McAuley DF, McKenna DH, Traber LD, Zhuo H, Wilson J, Herndon DN, Prough DS, Liu KD, Matthay MA, and Enkhbaatar P**. Human mesenchymal stem cells reduce the severity of acute lung injury in a sheep model of bacterial pneumonia. *Thorax* 69: 819-825, 2014.

4. **Dane DM, Yan X, Tamhane RM, Johnson RL, Jr., Estrera AS, Hogg DC, Hogg RT, and Hsia CCW**. Retinoic acid-induced alveolar cellular growth does not improve function after right pneumonectomy. *J Appl Physiol* 96: 1090-1096, 2004.

5. **Dane DM, Yilmaz C, Estrera AS, and Hsia CC**. Separating in vivo mechanical stimuli for postpneumonectomy compensation: physiological assessment. *J Appl Physiol (1985)* 114: 99-106, 2013.

6. **Dane DM, Yilmaz C, Gyawali D, Iyer R, Menon J, Nguyen KT, Ravikumar P, Estrera AS, and Hsia CCW**. Erythropoietin inhalation enhances adult canine alveolar-capillary formation following pneumonectomy. *Am J Physiol Lung Cell Mol Physiol* 316: L936-L945, 2019.

7. **Dane DM, Yilmaz C, Gyawali D, Iyer R, Ravikumar P, Estrera AS, and Hsia CC**. Perfusion-related stimuli for compensatory lung growth following pneumonectomy. *J Appl Physiol (1985)* 121: 312-323, 2016.

8. **Djonov V, Baum O, and Burri PH**. Vascular remodeling by intussusceptive angiogenesis. *Cell and Tissue Research* 314: 107-117, 2003.

9. **Eisenhauer P, Earle B, Loi R, Sueblinvong V, Goodwin M, Allen GB, Lundblad L, Mazan MR, Hoffman AM, and Weiss DJ**. Endogenous distal airway progenitor cells, lung mechanics, and disproportionate lobar growth following long-term postpneumonectomy in mice. *Stem Cells* 31: 1330-1339, 2013.

10. **Gazdhar A, Grad I, Tamo L, Gugger M, Feki A, and Geiser T**. The secretome of induced pluripotent stem cells reduces lung fibrosis in part by hepatocyte growth factor. *Stem Cell Res Ther* 5: 123, 2014.

11. **Gazdhar A, Ravikumar P, Pastor J, Heller M, Ye J, Zhang J, Moe OW, Geiser T, and Hsia CCW**. Alpha-Klotho Enrichment in Induced Pluripotent Stem Cell Secretome Contributes to Antioxidative Protection in Acute Lung Injury. *Stem Cells* 36: 616-625, 2018.

12. **Gennai S, Monsel A, Hao Q, Park J, Matthay MA, and Lee JW**. Microvesicles Derived From Human Mesenchymal Stem Cells Restore Alveolar Fluid Clearance in Human Lungs Rejected for Transplantation. *Am J Transplant* 15: 2404-2412, 2015.

13. **Golpanian S, DiFede DL, Pujol MV, Lowery MH, Levis-Dusseau S, Goldstein BJ, Schulman IH, Longsomboon B, Wolf A, Khan A, Heldman AW, Goldschmidt-Clermont PJ, and Hare JM**. Rationale and design of the allogeneiC human mesenchymal stem cells (hMSC) in patients with aging fRAilTy via intravenoUS delivery (CRATUS) study: A phase I/II, randomized, blinded and placebo controlled trial to evaluate the safety and potential efficacy of allogeneic human mesenchymal stem cell infusion in patients with aging frailty. *Oncotarget* 7: 11899-11912, 2016.

14. **Guimaraes-Fernandes F, Samano MN, Vieira RP, Carvalho CR, Pazetti R, Moreira LF, Pego-Fernandes PM, and Jatene FB**. Effect of methylprednisolone on perivascular pulmonary edema, inflammatory infiltrate, VEGF and TGF-beta immunoexpression in the remaining lungs of rats after left pneumonectomy. *Braz J Med Biol Res* 44: 647-651, 2011.

15. **Hao Q, Zhu YG, Monsel A, Gennai S, Lee T, Xu F, and Lee JW**. Study of Bone Marrow and Embryonic Stem Cell-Derived Human Mesenchymal Stem Cells for Treatment of Escherichia coli Endotoxin-Induced Acute Lung Injury in Mice. *Stem Cells Transl Med* 4: 832-840, 2015.

16. **Hogan BL, Barkauskas CE, Chapman HA, Epstein JA, Jain R, Hsia CC, Niklason L, Calle E, Le A, Randell SH, Rock J, Snitow M, Krummel M, Stripp BR, Vu T, White ES, Whitsett JA, and Morrisey EE**. Repair and regeneration of the respiratory system: complexity, plasticity, and mechanisms of lung stem cell function. *Cell Stem Cell* 15: 123-138, 2014.

17. **How CK, Chien Y, Yang KY, Shih HC, Juan CC, Yang YP, Chiou GY, Huang PI, Chang YL, Chen LK, Wang CY, Hsu HS, Chiou SH, and Lee CH**. Induced pluripotent stem cells mediate the release of interferon gamma-induced protein 10 and alleviate bleomycin-induced lung inflammation and fibrosis. *Shock* 39: 261-270, 2013.

18. **Hsia CC**. Comparative analysis of the mechanical signals in lung development and compensatory growth. *Cell Tissue Res* 367: 687-705, 2017.

19. **Hsia CC, Herazo LF, Ramanathan M, and Johnson RL, Jr.** Cardiopulmonary adaptations to pneumonectomy in dogs. IV. Membrane diffusing capacity and capillary blood volume. *J Appl Physiol (1985)* 77: 998-1005, 1994.

20. **Hsia CC, Herazo LF, Ramanathan M, Johnson RL, Jr., and Wagner PD**. Cardiopulmonary adaptations to pneumonectomy in dogs. II. VA/Q relationships and microvascular recruitment. *J Appl Physiol* 74: 1299-1309, 1993.

21. **Hsia CC, Hyde DM, Ochs M, Weibel ER, and ATS/ERS Joint Task Force on Quantitative Assessment of Lung Structure**. An official research policy statement of the American Thoracic Society/European Respiratory Society: standards for quantitative assessment of lung structure. *Am J Respir Crit Care Med* 181: 394-418, 2010.

22. **Hsia CC, and Ravikumar P**. Role of mechanical stress in lung repair and regeneration. In: *Stem cells in the lung, Chapter 12*, edited by Bertoncello I. Switzerland: Springer International, 2015, p. 191-212.

23. **Hsia CC, Wagner PD, Dane DM, Wagner HE, and Johnson RL, Jr.** Predicting diffusive alveolar oxygen transfer from carbon monoxide-diffusing capacity in exercising foxhounds. *J Appl Physiol (1985)* 105: 1441-1447, 2008.

24. **Kaza AK, Kron IL, Kern JA, Long SM, Fiser SM, Nguyen RP, Tribble CG, and Laubach VE**. Retinoic acid enhances lung growth after pneumonectomy. *Ann Thorac Surg* 71: 1645-1650, 2001.

25. **Kaza AK, Kron IL, Leuwerke SM, Tribble CG, and Laubach VE**. Keratinocyte growth factor enhances post-pneumonectomy lung growth by alveolar proliferation. *Circulation* 106: I120-124, 2002.

26. **Krause A, Xu Y, Joh J, Hubner R, Gess A, Ilic T, and Worgall S**. Overexpression of sonic Hedgehog in the lung mimics the effect of lung injury and compensatory lung growth on pulmonary Sca-1 and CD34 positive cells. *Mol Ther* 18: 404-412.

27. **Lee JW, Fang X, Gupta N, Serikov V, and Matthay MA**. Allogeneic human mesenchymal stem cells for treatment of E. coli endotoxin-induced acute lung injury in the ex vivo perfused human lung. *Proc Natl Acad Sci U S A* 106: 16357-16362, 2009.

28. **Mohammadipoor A, Antebi B, Batchinsky AI, and Cancio LC**. Therapeutic potential of products derived from mesenchymal stem/stromal cells in pulmonary disease. *Respir Res* 19: 218, 2018.

29. **Monsel A, Zhu YG, Gudapati V, Lim H, and Lee JW**. Mesenchymal stem cell derived secretome and extracellular vesicles for acute lung injury and other inflammatory lung diseases. *Expert Opin Biol Ther* 16: 859-871, 2016.

30. **Nolen-Walston RD, Kim CF, Mazan MR, Ingenito EP, Gruntman AM, Tsai L, Boston R, Woolfenden AE, Jacks T, and Hoffman AM**. Cellular kinetics and modeling of

bronchioalveolar stem cell response during lung regeneration. *Am J Physiol Lung Cell Mol Physiol* 294: L1158-1165, 2008.

31. **Paxson JA, Gruntman AM, Davis AM, Parkin CM, Ingenito EP, and Hoffman AM**. Age dependence of lung mesenchymal stromal cell dynamics following pneumonectomy. *Stem Cells Dev* 22: 3214-3225, 2013.

32. **Pengelly LD**. Curve-fitting analysis of pressure-volume characteristics of the lungs. *Journal of Applied Physiology* 42: 111-116, 1977.

33. **Pierog J, Fytianos K, Tamo L, Simillion C, Taddeo A, Kocher G, Gugger M, Grodzki T, Heller M, Blank F, Geiser T, Schmid RA, and Gazdhar A**. Stem cell secretome attenuates acute rejection in rat lung allotransplant. *Interact Cardiovasc Thorac Surg* 28: 812-818, 2019.

34. **Ravikumar P, Dane DM, McDonough P, Yilmaz C, Estrera AS, and Hsia CC**. Long-term post-pneumonectomy pulmonary adaptation following all-trans-retinoic acid supplementation. *Journal of Applied Physiology* 110: 764-773, 2011.

35. **Ravikumar P, Li L, Ye J, Shi M, Taniguchi M, Zhang J, Kuro-o M, Hu MC, Moe OW, and Hsia CC**. alphaKlotho deficiency in acute kidney injury contributes to lung damage. *J Appl Physiol (1985)* 120: 723-732, 2016.

36. **Ravikumar P, Ye J, Zhang J, Pinch SN, Hu MC, Kuro-o M, Hsia CC, and Moe OW**. alpha-Klotho protects against oxidative damage in pulmonary epithelia. *Am J Physiol Lung Cell Mol Physiol* 307: L566-575, 2014.

37. **Ravikumar P, Yilmaz C, Bellotto DJ, Dane DM, Estrera AS, and Hsia CC**. Separating in vivo mechanical stimuli for postpneumonectomy compensation: imaging and ultrastructural assessment. *J Appl Physiol (1985)* 114: 961-970, 2013.

38. **Ravikumar P, Yilmaz C, Dane DM, Bellotto DJ, Estrera AS, and Hsia CC**. Defining a stimuli-response relationship in compensatory lung growth following major resection. *J Appl Physiol (1985)* 116: 816-824, 2014.

592 39. **Roughton FJ, and Forster RE**. Relative importance of diffusion and chemical reaction
593 rates in determining the rate of exchange of gases in the human lung, with special reference to
594 true diffusing capacity of pulmonary membrane and volume of blood in the lung capillaries. *J*
595 *Appl Physiol* 11: 290-302, 1957.
596 40. **Sakurai MK, Lee S, Arsenault DA, Nose V, Wilson JM, Heymach JV, and Puder M**.
597 Vascular endothelial growth factor accelerates compensatory lung growth after unilateral
598 pneumonectomy. *American Journal of Physiology Lung Cell and Molecular Physiology* 292:
599 L742-747, 2007.
600 41. **Salazar E, and Knowles JH**. An Analysis of Pressure-Volume Characteristics of the
601 Lungs. *J Appl Physiol* 19: 97-104, 1964.
602 42. **Song L, Xu J, Qu J, Sai Y, Chen C, Yu L, Li D, and Guo X**. A therapeutic role for
603 mesenchymal stem cells in acute lung injury independent of hypoxia-induced mitogenic factor. *J*
604 *Cell Mol Med* 16: 376-385, 2012.
605 43. **Steens J, and Klein D**. Current Strategies to Generate Human Mesenchymal Stem
606 Cells In Vitro. *Stem Cells Int* 2018: 6726185, 2018.
607 44. **Tamo L, Simillion C, Hibaoui Y, Feki A, Gugger M, Prasse A, Jager B, Goldmann T,**
608 **Geiser T, and Gazdhar A**. Gene Network Analysis of Interstitial Macrophages After Treatment
609 with Induced Pluripotent Stem Cells Secretome (iPSC-cm) in the Bleomycin Injured Rat Lung.
610 *Stem Cell Rev Rep* 14: 412-424, 2018.
611 45. **Tan Y, Ooi S, and Wang L**. Immunogenicity and tumorigenicity of pluripotent stem cells
612 and their derivatives: genetic and epigenetic perspectives. *Curr Stem Cell Res Ther* 9: 63-72,
613 2014.
614 46. **Wang Y, Zhang L, Li Y, Chen L, Wang X, Guo W, Zhang X, Qin G, He SH,**
615 **Zimmerman A, Liu Y, Kim IM, Weintraub NL, and Tang Y**. Exosomes/microvesicles from
616 induced pluripotent stem cells deliver cardioprotective miRNAs and prevent cardiomyocyte
617 apoptosis in the ischemic myocardium. *Int J Cardiol* 192: 61-69, 2015.

618 47. **Wang YY, Li XZ, and Wang LB**. Therapeutic implications of mesenchymal stem cells in
619 acute lung injury/acute respiratory distress syndrome. *Stem Cell Res Ther* 4: 45, 2013.
620 48. **Weibel ER, Federspiel WJ, Fryder-Doffey F, Hsia CC, Konig M, Stalder-Navarro V,**
621 **and Vock R**. Morphometric model for pulmonary diffusing capacity. I. Membrane diffusing
622 capacity. *Respir Physiol* 93: 125-149, 1993.
623 49. **Willis GR, Fernandez-Gonzalez A, Anastas J, Vitali SH, Liu X, Ericsson M, Kwong**
624 **A, Mitsialis SA, and Kourembanas S**. Mesenchymal Stromal Cell Exosomes Ameliorate
625 Experimental Bronchopulmonary Dysplasia and Restore Lung Function through Macrophage
626 Immunomodulation. *Am J Respir Crit Care Med* 197: 104-116, 2018.
627 50. **Yan X, Bellotto DJ, Dane DM, Elmore RG, Johnson RL, Jr., Estrera AS, and Hsia**
628 **CC**. Lack of response to all-trans retinoic acid supplementation in adult dogs following left
629 pneumonectomy. *J Appl Physiol* 99: 1681-1688, 2005.
630 51. **Yan X, Bellotto DJ, Foster DJ, Johnson RL, Jr., Hagler HH, Estrera AS, and Hsia**
631 **CC**. Retinoic acid induces nonuniform alveolar septal growth after right pneumonectomy. *J Appl*
632 *Physiol* 96: 1080-1089, 2004.
633 52. **Yan X, Polo Carbayo JJ, Weibel ER, and Hsia CC**. Variation of lung volume after
634 fixation when measured by immersion or Cavalieri method. *Am J Physiol Lung Cell Mol Physiol*
635 284: L242-245, 2003.
636 53. **Yang KY, Shih HC, How CK, Chen CY, Hsu HS, Yang CW, Lee YC, Perng RP, Peng**
637 **CH, Li HY, Chang CM, Mou CY, and Chiou SH**. IV delivery of induced pluripotent stem cells
638 attenuates endotoxin-induced acute lung injury in mice. *Chest* 140: 1243-1253, 2011.
639 54. **Yilmaz C, Dane DM, Tustison N, Song G, Gee JC, and Hsia CCW**. In vivo imaging of
640 canine lung deformation: Effects of posture, pneumonectomy, and inhaled erythropoietin. *J Appl*
641 *Physiol (1985)* doi: 10.1152/japplphysiol.00647.02019 [Epub ahead of print], 2020.

55. **Yilmaz C, Ravikumar P, Dane DM, Bellotto DJ, Johnson RL, Jr., and Hsia CC**. Noninvasive quantification of heterogeneous lung growth following extensive lung resection by high-resolution computed tomography. *J Appl Physiol* 107: 1569-1578, 2009.

56. **Yilmaz C, Tustison NJ, Dane DM, Ravikumar P, Takahashi M, Gee JC, and Hsia CC**. Progressive adaptation in regional parenchyma mechanics following extensive lung resection assessed by functional computed tomography. *Journal of Applied Physiology* 111: 1150-1158, 2011.

57. **Yuan S, Hannam V, Belcastro R, Cartel N, Cabacungan J, Wang J, Diambomba Y, Johnstone L, Post M, and Tanswell AK**. A role for platelet-derived growth factor-BB in rat postpneumonectomy compensatory lung growth. *Pediatr Res* 52: 25-33, 2002.

58. **Zhang J, Cao K, Pastor JV, Li L, Moe OW, and Hsia CCW**. Alpha-Klotho, a critical protein for lung health, is not expressed in normal lung. *FASEB Bioadv* 1: 675-687, 2019.

59. **Zhang Q, Bellotto DJ, Ravikumar P, Moe OW, Hogg RT, Hogg DC, Estrera AS, Johnson RL, Jr., and Hsia CC**. Postpneumonectomy lung expansion elicits hypoxia-inducible factor-1alpha signaling. *Am J Physiol Lung Cell Mol Physiol* 293: L497-504, 2007.

Figure legend

Figure 1. Timeline of the studies. CFM: cell-free media; iPSC CM: iPSC conditioned media.

Figure 2. Lung volume-transpulmonary pressure relationship pre- and post-PNX. Lung volume at a given transpulmonary pressure was similarly lower post-PNX compared to pre-PNX in animals treated with cell-free media (CFM) or iPSC conditioned media (iPSC CM). Mean ± SD. Repeated measures ANOVA. Number of animals: 5 CFM, 6 iPSC CM.

Figure 3. Lung function pre- and post-PNX in animals treated with cell-free media (CFM) or iPSC conditioned media (iPSC CM)**. A.** End-inspiratory lung volume (EILV). **B.** End-expiratory lung volume (EELV). **C.** Pulmonary blood flow. **D.** DL_{CO} measured at an inflation volume of 45 $ml \cdot kg^{-1}$ and inspired O_2 concentration of 21% was expressed under standard conditions (hematocrit = 0.45, alveolar PO_2 =120 mmHg). **E.** Membrane diffusing capacity **(**DM_{CO}). **F.** pulmonary capillary blood volume (Vc). Box: Mean ± SD; whiskers extend to maximum and minimum values. Factorial and repeated measures ANOVA. Number of animals: 5 CFM, 6 iPSC CM.

Figure 4. **Changes (post/pre-PNX ratio) in plasma biomarkers. (A)** 8-hydroxy-2'-deoxyguanosine (8-OHdG)**, (B)** 8-isoprostane**,** and **(C)** total antioxidant capacity (copper reducing equivalents) in animals treated with cell-free media (CFM) or iPSC conditioned media (iPSC CM). Mean ± SD. Symbols for p<0.0.5 with respect to time post-PNX: † vs. Pre-PNX, ‡ vs. 1 h post-PNX (0 d), § vs. 5 d, # vs. 10 d, @ vs. 20 d, ¶ vs. 30 d, $ vs. 40 d by factorial ANOVA. Overall comparison between treatment groups by repeated measures ANOVA: (**A**) p=0.69, (**B**) p=0.39, and (**C**) p=0.25. Number of animals: 5 CFM, 6 iPSC CM.

Figure 5. Representative distal lung morphology under light and electron microscopy in post-PNX animals treated with cell-free media (CFM) or iPSC conditioned media (iPSC CM),

681 illustrating a thinner septal tissue layer in iPSC CM group on the “thin side” of the blood-gas
682 barrier where the bulk of alveolar gas exchange takes place. Top panels: bar = 50 μm. Lower
683 panels: bar = 2 μm.

684 **Figure 6. Morphometric results** in the left caudal lobe in post-PNX animals treated with cell-
685 free media (CFM) or iPSC conditioned media (iPSC CM). (**A**) Total lobe volume (intact or serial
686 sectioned). (**B**) Volume of alveolar sacs and ducts. (**C**) Alveolar surface area. (**D**) Prevalence of
687 alveolar double capillary profiles. Box: Mean ± SD; whiskers extend to maximum and minimum
688 values. P values indicate iPSC CM vs. CFM by unpaired t-test. Five animals per group.

689 **Figure 7. Frequency distribution of harmonic mean thickness of the tissue-plasma barrier**
690 in post-PNX animals treated with cell-free media (CFM) or iPSC conditioned media (iPSC CM).
691 Box: Mean ± SD; whiskers extend to maximum and minimum values. P values shown indicate
692 iPSC CM vs. CFM in each barrier thickness category by unpaired t-test. Overall comparison
693 between treatment groups by repeated measures ANOVA (p=0.16). Five animals per group.
694

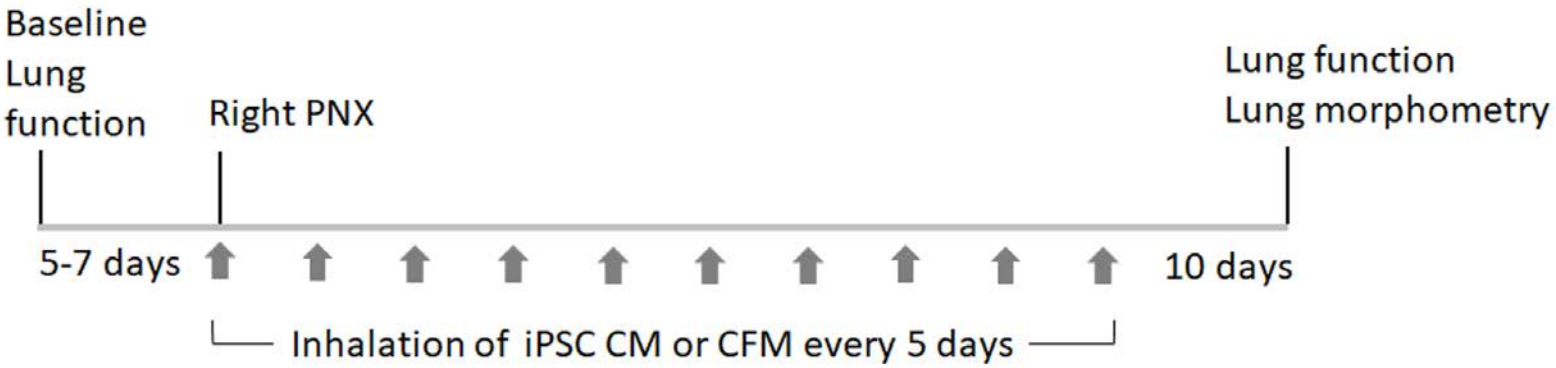

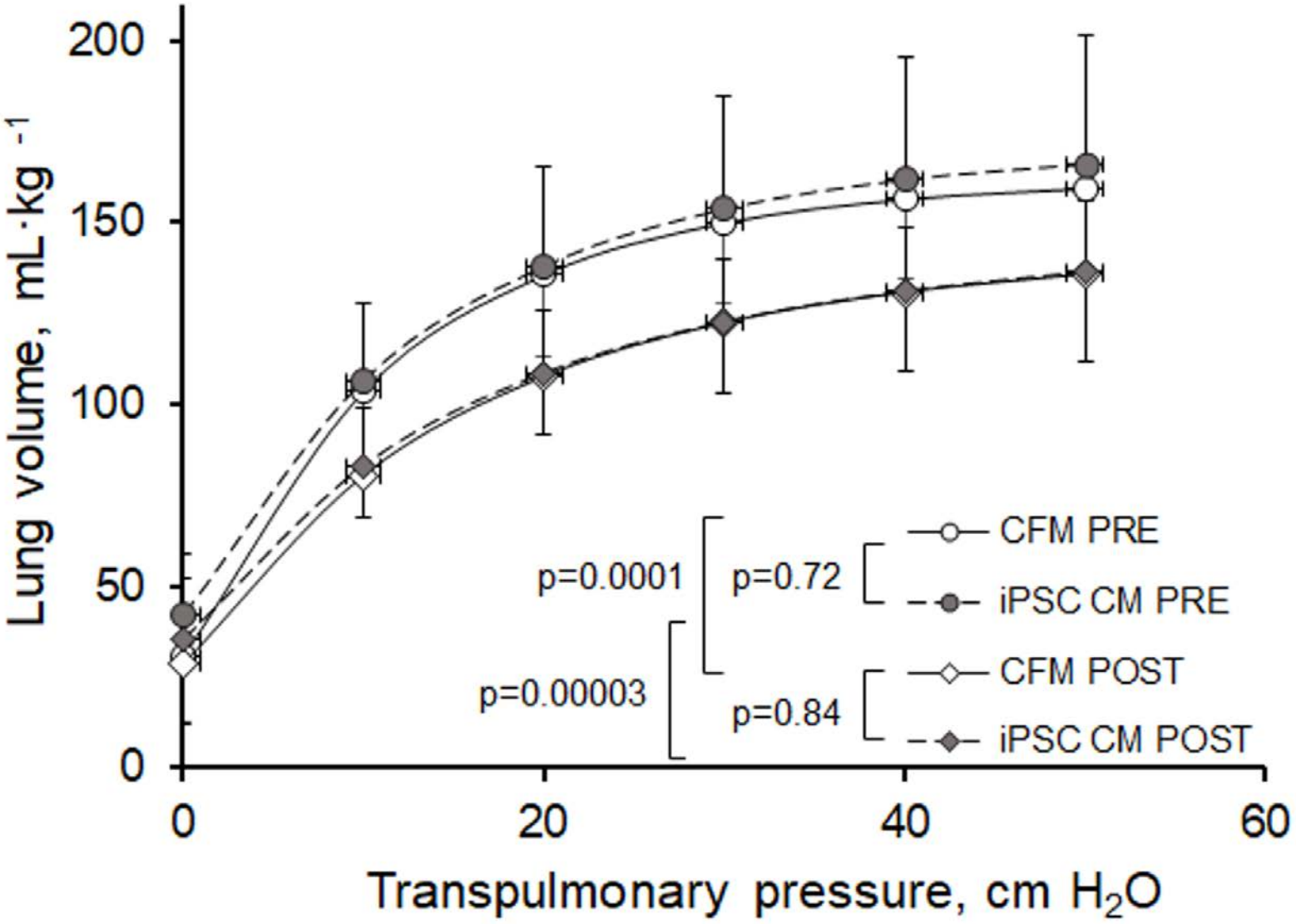

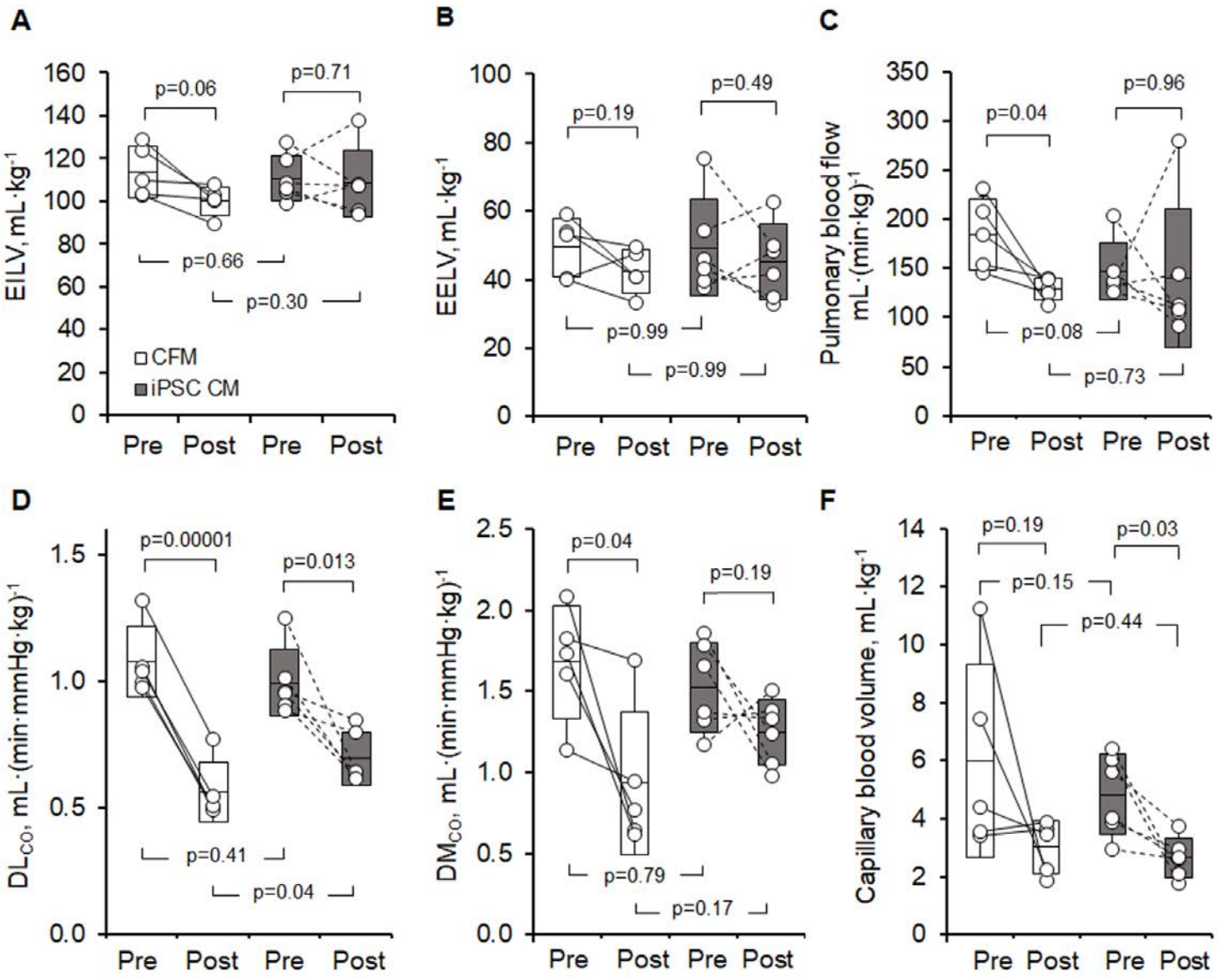

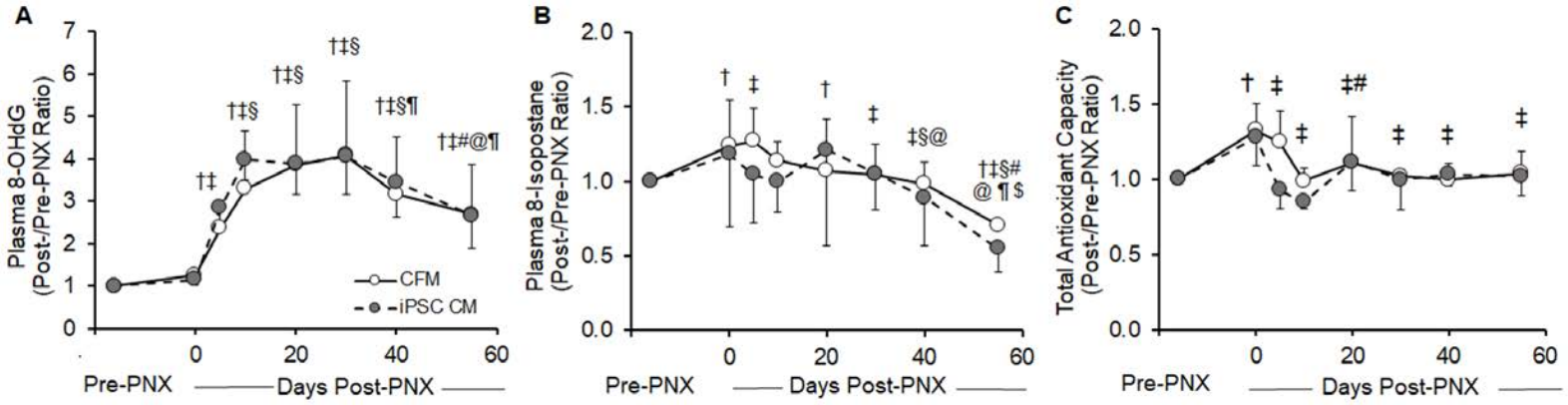

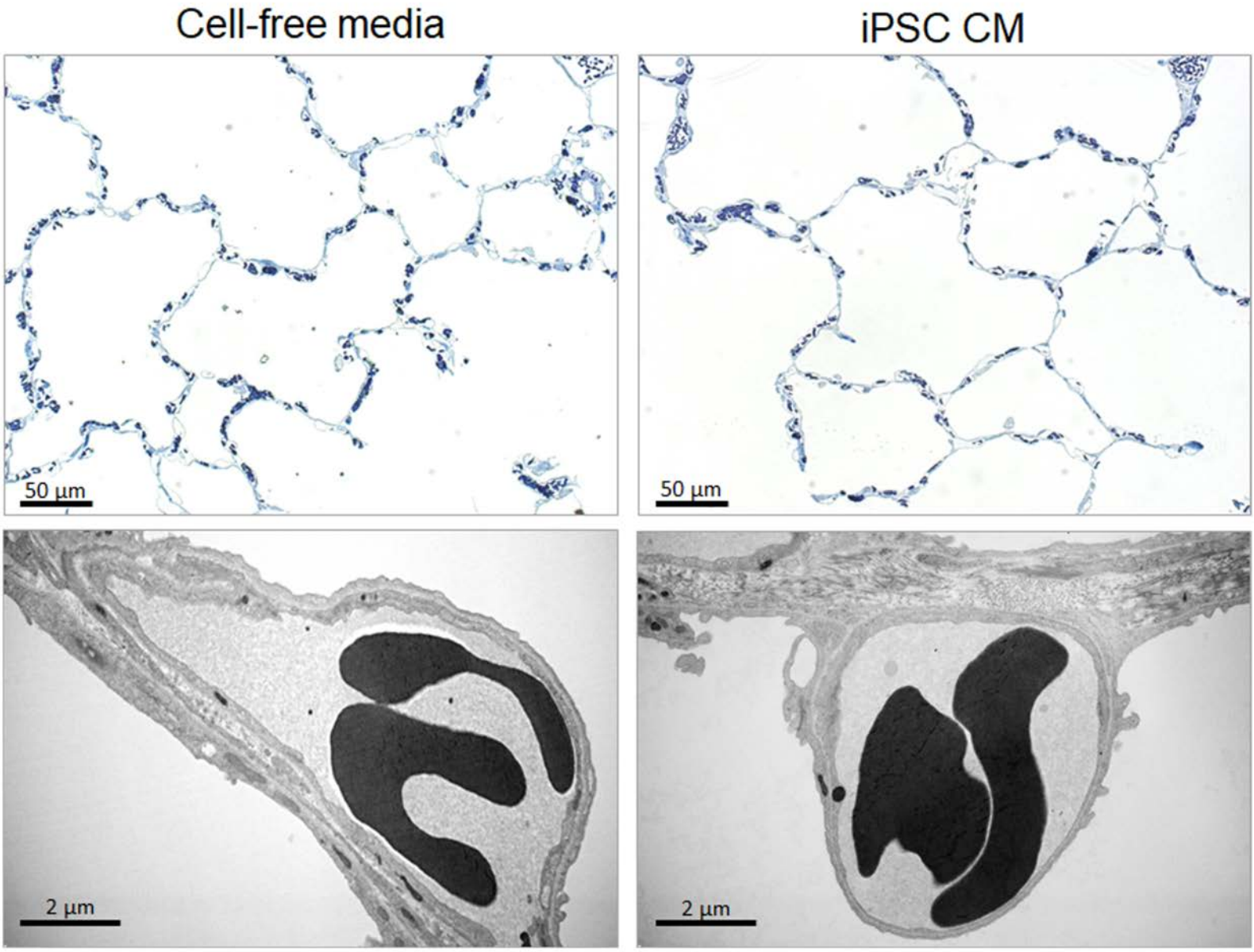

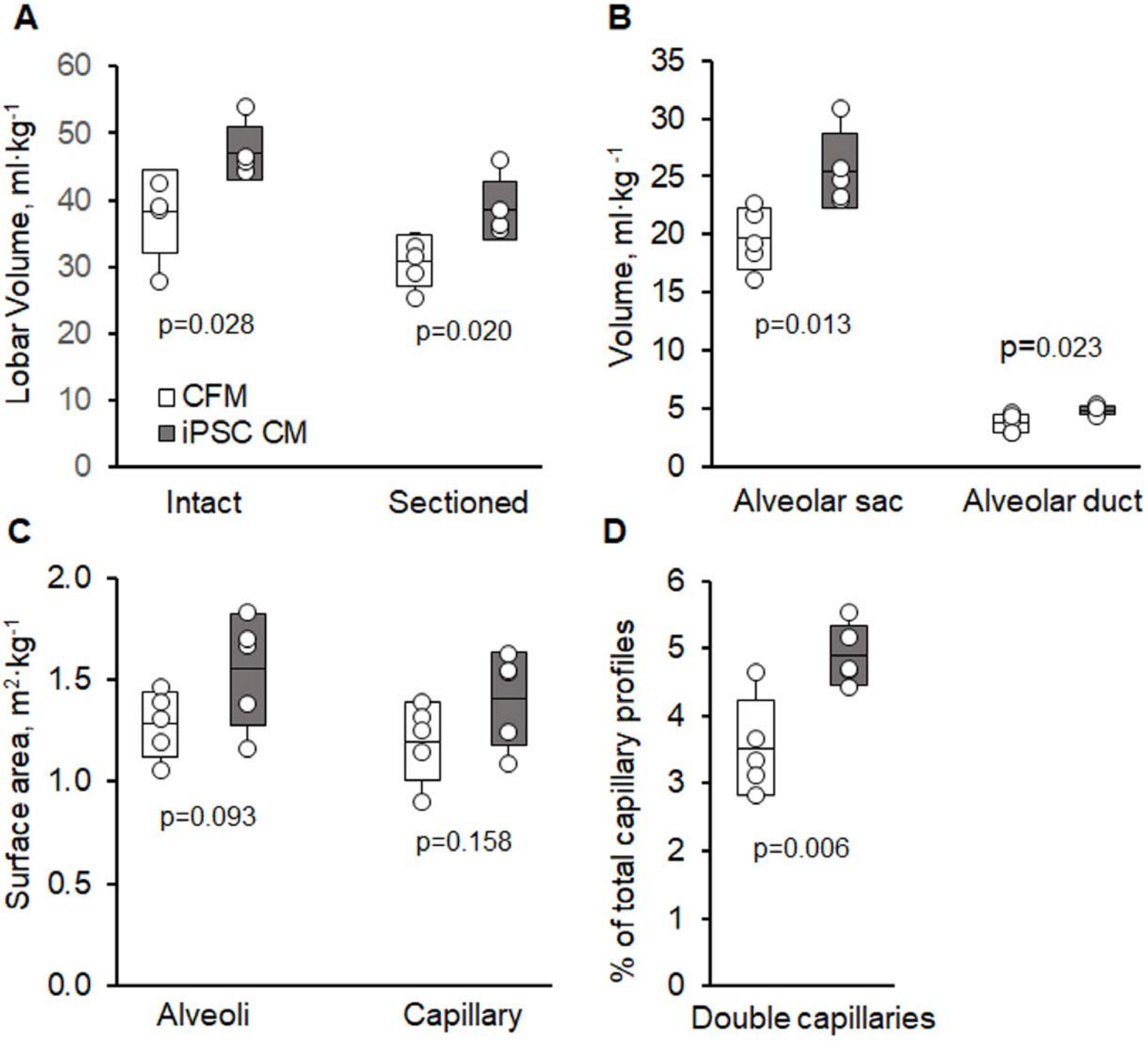

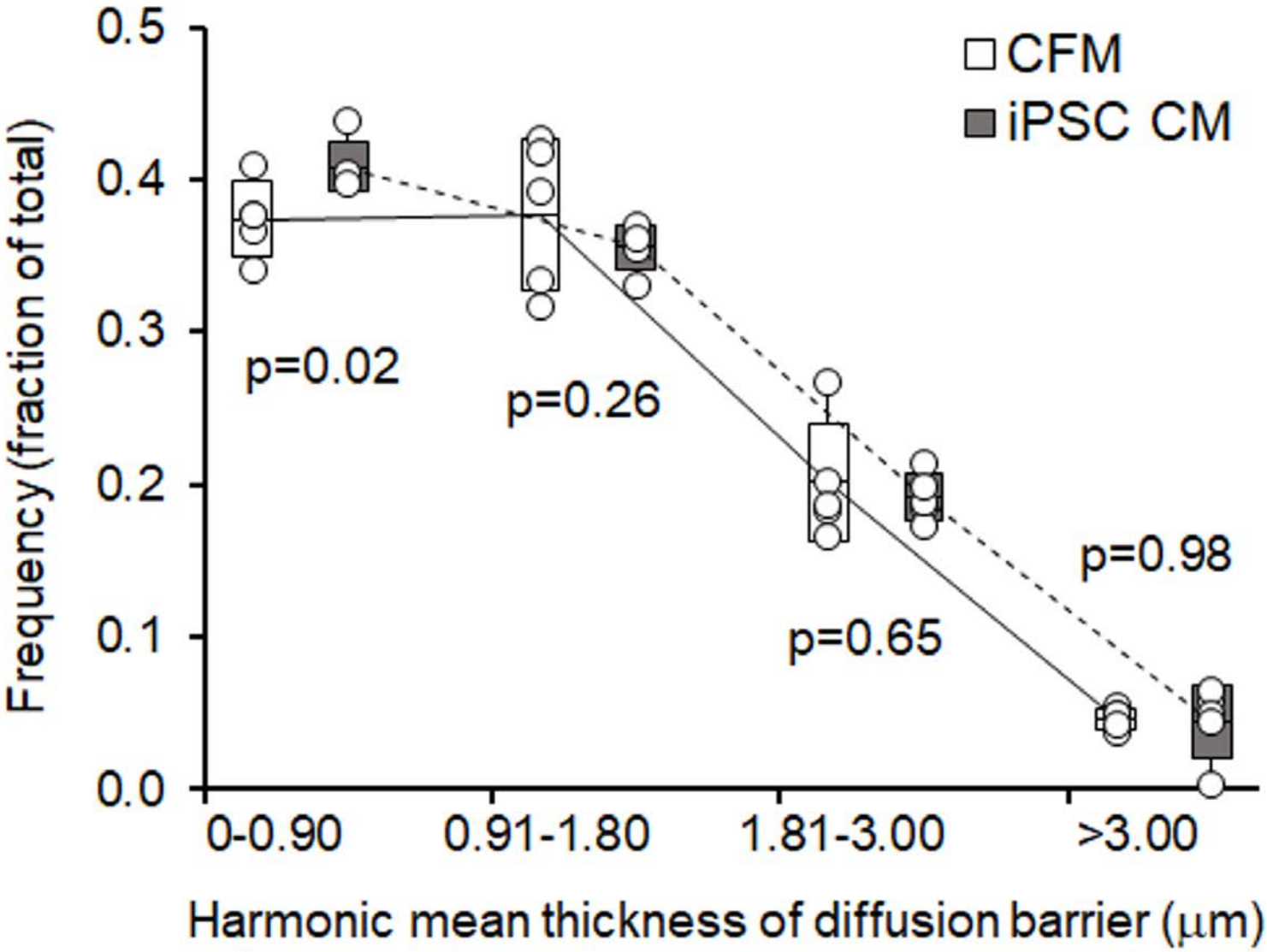

Table 1. Lung function

Group	CFM		iPSC CM		P value		
PNX	PRE-PNX	POST-PNX	PRE-PNX	POST-PNX	vs. Group	vs. PNX	Group*PNX
N	5	5	6	6			
Body weight, kg	18.4 ± 1.6	18.5 ± 2.1	18.2 ± 0.3	18.5 ± 1.8	0.87	0.78	0.83
Hematocrit, %, sedated	42.8 ± 1.8	39.9 ± 3.2	42.0 ± 2.7	40.0 ± 2.8	0.78	0.048	0.68
Specific lung compliance, mL·(cmH_2O·L)$^{-1}$	23.0 ± 5.8	27.7 ± 5.9	22.0 ± 2.4	24.5 ± 5.1	0.32	0.13	0.63
Alveolar PO_2 breathing 21% O_2, mm Hg	125.3 ± 36.4	129.3 ± 19.5	128.8 ± 30.9	135.9 ± 18.5	0.70	0.60	0.88
Alveolar PO_2 breathing 99% O_2, mm Hg	664.7 ± 14.3	669.9 ± 4.0	663.1 ± 4.8	670.1 ± 4.4	0.86	0.12	0.77
End-expiratory lung volume, mL·kg^{-1}	55.7 ± 11.9	49.0 ± 9.1	52.5 ± 10.6	50.1 ± 16.4	0.85	0.38	0.67
End-inspiratory lung volume, mL·kg^{-1}	113.8 ± 12.0	100.2 ± 6.8 #	110.7 ± 10.6	108.4 ± 15.6	0.68	0.08	0.19
Pulmonary blood flow, mL·(min·kg)$^{-1}$	184.5 ± 35.8	129.2 ± 11.6 †	146.8 ± 28.8	140.4 ± 70.8	0.45	0.17	0.26
DL_{NO}, mL·(min·mm Hg·kg)$^{-1}$	3.46 ± 1.25	2.61 ± 0.46	3.22 ± 0.54	2.58 ± 0.64	0.65	0.07	0.78
DL_{CO} measured, mL·(min·mm Hg·kg)$^{-1}$	1.01 ± 0.16	0.50 ± 0.06 †	0.87 ± 0.04	0.58 ± 0.11 †	0.60	<.0001 †	0.004 ‡
$DL_{CO\text{-}std}$, mL·(min·mm Hg·kg)$^{-1}$	1.08 ± 0.14	0.56 ± 0.12 †	0.99 ± 0.13	0.69 ± 0.10 *†	0.71	<.0001 †	0.04 ‡
DM_{CO}, mL·(min·mm Hg·kg)$^{-1}$	1.68 ± 0.35	0.93 ± 0.44 †	1.53 ± 0.28	1.25 ± 0.20	0.51	0.01 †	0.17
Capillary blood volume, mL·kg^{-1}	6.00 ± 3.34	3.03 ± 0.91	4.82 ± 1.38	2.65 ± 0.69 †	0.22	0.02 †	0.68
Septal tissue volume, mL·kg^{-1}	6.62 ± 1.70	6.60 ± 2.65	5.96 ± 3.01	6.14 ± 3.85	0.66	0.95	0.94

Mean±SD. Repeated measures ANOVA: * p<0.05 vs. CFM group post-PNX. † p<0.05, # p=0.06 vs. corresponding Pre-PNX group. ‡ p<0.05 Group*PNX interaction. Specific lung compliance was measured at transpulmonary pressure between 10 and 30 cm H_2O, normalized by lung volume at 10 cm H_2O. DL_{CO} was measured at 45 mL/kg inflation volume. $DL_{CO\text{-}std}$: results were expressed at standardized conditions (hematocrit = 0.45 and alveolar PO_2 =120 mmHg).

Table 2. Morphometric Data

	CFM	iPSC CM	P value
Number of animals	5	5	
Terminal body weight (kg)	18.5 ± 2.1	18.6 ± 1.9	0.902
Total lobar volume, $mL \cdot kg^{-1}$			
Intact (Immersion method)	38.2 ± 6.2	47.0 ± 4.0	* 0.028
Sectioned (Cavalieri method)	30.9 ± 3.9	38.5 ± 4.3	* 0.020
Morphometric hematocrit, %	43.0 ± 2.4	44.4 ± 2.4	0.357
Arithmetic mean septal thickness, μm	4.73 ± 0.56	4.41 ± 0.49	0.356
Harmonic mean barrier thickness, (τ_{hb}), μm	0.97 ± 0.03	0.92 ± 0.03	* 0.046
Double capillary profiles, %	3.52 ± 0.70	4.90 ± 0.44	* 0.006

Mean±SD. * $p<0.05$ iPSC CM vs. CFM by unpaired t test.

Table 3. Volume-to-Volume and surface-to-volume ratios of alveolar structures

	CFM	iPSC CM		p value
	Volume per unit lung volume			
Coarse parenchyma	0.8870 ± 0.0234	0.9039 ± 0.0154		0.213
Fine parenchyma	0.8723 ± 0.0225	0.8914 ± 0.0133		0.141
Respiratory bronchioles	0.0286 ± 0.0096	0.0292 ± 0.0049		0.904
Alveolar sac	0.6370 ± 0.0165	0.6620 ± 0.0148	*	0.035
Alveolar duct	0.1211 ± 0.0175	0.1267 ± 0.0079		0.536
Septum (tissue+blood)	0.0982 ± 0.0095	0.0886 ± 0.0141		0.246
Total epithelium	0.0166 ± 0.0011	0.0156 ± 0.0027		0.467
Type I epithelium	0.0101 ± 0.0012	0.0094 ± 0.0022		0.555
Type II epithelium	0.0065 ± 0.0005	0.0062 ± 0.0015		0.677
Interstitium	0.0232 ± 0.0048	0.0210 ± 0.0037		0.438
Collagen fibers	0.0184 ± 0.0031	0.0163 ± 0.0032		0.320
Cells and matrix	0.0049 ± 0.0022	0.0048 ± 0.0011		0.924
Endothelium	0.0118 ± 0.0022	0.0122 ± 0.0031		0.828
Septal Extravascular tissue	0.0517 ± 0.0068	0.0489 ± 0.0087		0.583
Capillaries	0.0465 ± 0.0136	0.0398 ± 0.0093		0.391
	Surface area per unit lung volume, cm^{-1}			
Alveolar Surface	416 ± 18	403 ± 57		0.643
Capillary Surface	387 ± 24	366 ± 51		0.428

Mean±SD. * p<0.05 IPS vs. CFM by unpaired t test.

Table 4. Absolute volumes, surface areas, and conductance for oxygen

	CFM	iPSC CM	P value
	Volume, ml·kg^{-1}		
Coarse parenchyma	27.41 ± 3.87	34.80 ± 4.16	* 0.020
Fine parenchyma	26.96 ± 3.80	34.32 ± 4.09	* 0.018
Alveolar sac	19.67 ± 2.64	25.49 ± 3.16	* 0.013
Alveolar duct	3.75 ± 0.78	4.86 ± 0.41	* 0.023
Respiratory bronchioles	0.89 ± 0.31	1.13 ± 0.24	0.212
Septum	3.04 ± 0.58	3.40 ± 0.54	0.348
Total epithelium	0.51 ± 0.08	0.61 ± 0.15	0.253
Type I	0.31 ± 0.06	0.36 ± 0.10	0.369
Type II	0.20 ± 0.02	0.24 ± 0.08	0.260
Interstitium	0.72 ± 0.18	0.81 ± 0.14	0.409
Collagen fibers	0.57 ± 0.13	0.62 ± 0.12	0.496
Cells and matrix	0.15 ± 0.07	0.18 ± 0.04	0.385
Endothelium	0.36 ± 0.06	0.47 ± 0.14	0.155
Extravascular tissue	1.59 ± 0.28	1.88 ± 0.41	0.224
Capillaries	1.45 ± 0.54	1.51 ± 0.29	0.825
	Surface area, m^2·kg^{-1}		
Alveolar surface	1.28 ± 0.16	1.55 ± 0.27	0.093
Capillary surface	1.20 ± 0.19	1.41 ± 0.23	0.158
O_2 conductance of tissue-plasma barrier (Db_{O2}), mL·(min·mmHg·kg)$^{-1}$	1.95 ± 0.29	2.46 ± 0.46	0.068

Mean±SD. * p<0.05 iPSC CM vs. CFM by unpaired t test.